PAPER

Iron(III) carboxylate/aminoalcohol coordination clusters with propeller-shaped Fe$_8$ cores: approaching reasonable exchange energies†

Olga Botezat,[a,b] Jan van Leusen,[b] Victor Ch. Kravtsov,[a] Arkady Ellern,[c] Paul Kögerler*[b] and Svetlana G. Baca*[a]

A series of new octanuclear propeller-like aminoalcohol-supported Fe(III) oxocarboxylate coordination clusters, [Fe$_8$O$_3$(O$_2$CCHMe$_2$)$_9$(tea)(teaH)$_3$]·MeCN·2(H$_2$O) (**1**), [Fe$_8$O$_3$(O$_2$CCHMe$_2$)$_6$(N$_3$)$_3$(tea)(teaH)$_3$] (**2**), [Fe$_8$O$_3$(O$_2$CCMe$_3$)$_6$(N$_3$)$_3$(tea)(teaH)$_3$]·0.5(EtOH) (**3**), and [Fe$_8$O$_3$(O$_2$CCHMe$_2$)$_6$(N$_3$)$_3$(mdea)$_3$(MeO)$_3$] (**4**) (where teaH$_3$ = triethanolamine; mdeaH$_2$ = N-methyldiethanolamine) has been isolated and magneto-chemically analyzed combining the programs wxJFinder and CONDON in an approach to avoid overpara-meterization issues that are common to larger spin polytopes. Dominant antiferromagnetic exchange interactions exist in all clusters along the edges of the propellers, while moderate ferromagnetic inter-actions are found along the propeller axes in their {Fe$_8$O$_3$} metallic cores.

Introduction

Nanosized iron coordination clusters are attractive research targets in the fields of materials chemistry and physics due to their magnetic properties and great potential for application in "intelligent" multifunctional materials for information storage and quantum computation.[1] The number of metal ions in such clusters can be controlled through a proper choice of bridging ligands, which will act as intra- and/or intermolecular connectors and supply superexchange pathways between metal ions. Flexible polydentate N-donor alcohol ligands have been shown to progenerate numerous polynuclear nanosized coordination clusters, including several that show unusual magnetic behavior, as reported by us[2–4] and other groups.[5–9]

Although high-spin Fe^{III} nuclei in (distorted) octahedral ligand fields are readily described as pure spin-5/2 centers, the magnetic characteristics of polynuclear Fe^{III} clusters are increasingly complicated with each additional center. This is due to the growing number of structurally inequivalent nuclei and the proliferation of exchange pathways (n centers, $n(n − 1)/2$

pathways). We have recently demonstrated that in the case of μ_{2+m}-O-bridged Fe^{III} centers, the angular overlap model (AOM) can reliably assess inter- and intra-cluster interactions in hexa-nuclear Fe^{III} pivalate clusters [Fe$_6$O$_2$(O$_2$CH$_2$)(O$_2$CCMe$_3$)$_{12}$] bridged into 1D chains by 1,4-dioxane or 4,4′-bipyridine spacers.[10] To obtain reasonable initial values of the exchange coupling constants for the fitting routines of CONDON 2.0,[11] we introduced the program wxJFinder,[10,12] which combines AOM and structural information by extending the concepts of Weihe et al.[13a] and Werner et al.[13b] We herein demonstrate this approach on more complex Fe^{III} spin systems consisting of eight metal centers. For this purpose we prepared a series of new disk-like iron(III) oxocarboxylate cluster compounds of composition [Fe$_8$O$_3$(O$_2$CCHMe$_2$)$_9$(tea)(teaH)$_3$]·MeCN·2(H$_2$O) (**1**), [Fe$_8$O$_3$(O$_2$CCHMe$_2$)$_6$(N$_3$)$_3$(tea)(teaH)$_3$] (**2**), [Fe$_8$O$_3$(O$_2$CC-Me$_3$)$_6$(N$_3$)$_3$(tea)(teaH)$_3$]·0.5(EtOH) (**3**) and [Fe$_8$O$_3$(O$_2$CCH-Me$_2$)$_6$(N$_3$)$_3$(mdea)$_3$(MeO)$_3$] (**4**). These were synthesized by the reaction of smaller μ_3-oxo-centered trinuclear Fe^{III} carboxylate precursors, [Fe$_3$O(O$_2$CCHMe$_2$)$_6$(H$_2$O)$_3$]NO$_3$·2(MeCN)·2(H$_2$O) (**5**) or [Fe$_3$O(O$_2$CCMe$_3$)$_6$(H$_2$O)$_3$](Me$_3$CCO$_2$H)·2(Me$_3$CCO$_2$H),[14] with triethanolamine (teaH$_3$) or N-methyldiethanolamine (mdeaH$_2$) under various reaction conditions. Christou et al.[15] reported the first similar {Fe$_8$} benzoate cluster with teaH$_3$, [Fe$_8$O$_3$(O$_2$CPh)$_9$(tea)(teaH)$_3$]·MeCN, and this motif has been extended by Murray et al.[16] and Powell et al.[17] to a series of {Fe$_8$} disk-like propionate and pivalate clusters of the general formula [Fe$_8$O$_3$(O$_2$CR)$_6$(tea)(teaH)$_3$(L)$_3$]·solvent, where R = CH$_2$Me, L = F;[16] R = CMe$_3$, L = N$_3$ or SCN.[17] The flexibility of teaH$_3$ ligands has been explored by the groups of Wang and Gao[18] in the preparation of an {Fe$_{64}$} cluster consisting of eight octanuclear [Fe$_8$O$_3$(O$_2$CH)$_6$(tea)(teaH)$_3$] units. Using the mixed-

^{a}*Institute of Applied Physics, Academy of Science of Moldova, MD2028 Chisinau, R. Moldova. E-mail: sbaca_md@yahoo.com; Fax: +373-22-738154; Tel: +373-22-725887*

^{b}*Institute of Inorganic Chemistry, RWTH Aachen University, 52074 Aachen, Germany. E-mail: paul.koegerler@ac.rwth-aachen.de; Fax: +49-241-80-92642; Tel: +49-241-80-93642*

^{c}*Department of Chemistry, Iowa State University, Ames, IA 50011, USA*

ligand system of flexible teaH$_3$ and phenolic oxime, *e.g.* salicyl-aldoxime and its derivatives, Brechin *et al.*[19] have synthesized a series of {Fe$_8$} acetate clusters with similar metallic cores, [Fe$_8$O$_3$(O$_2$CMe)(R-sao)$_3$(tea)(teaH)$_3$] (R = Me, Et, and Ph).

Experimental

Materials and methods

All reactions were carried out under aerobic conditions using commercial grade solvents. [Fe$_3$O(O$_2$CCMe$_3$)$_6$(H$_2$O)$_3$]-(Me$_3$CCO$_2$)·2(Me$_3$CCO$_2$H) was prepared as reported elsewhere.[14] [Fe$_3$O(O$_2$CCHMe$_2$)$_6$(H$_2$O)$_3$]NO$_3$·2(MeCN)·2(H$_2$O) (**5**) was prepared as follows: 30 g of Fe(NO$_3$)$_3$·9H$_2$O in 30 mL of isobutyric acid were heated until the volume of the mixture was reduced by approximately 2/3, and then 50 mL of ethanol was added. The dark brown precipitate was filtered off after several days, washed with hexane and dried in air. The crystals of **5** suitable for X-ray measurements were grown from aceto-nitrile solution at −29 °C. Crystal data for **5**: C$_{28}$H$_{58}$Fe$_3$N$_3$O$_{21}$, M_r = 940.32 g mol^{-1}, triclinic, space group $P\bar{1}$, a = 11.990(7), b = 14.048(8), c = 14.837(8) Å, α = 76.891(10)°, β = 70.477(10)°, γ = 71.267(10)°, V = 2210.6(2) Å^3, Z = 2, R_1 = 0.0399 ($I > 2\sigma(I)$), wR_2 = 0.1040 (for 11 721 unique reflections and 527 refined parameters). Elemental analysis calcd for **5** without aceto-nitrile molecules, C$_{24}$H$_{52}$Fe$_3$NO$_{21}$: C, 33.56; H, 6.11; N, 1.63%. Found: C, 33.79; H, 5.87; N, 1.56%. IR (KBr pellet): ν = 3423 (m), 2969 (m), 2929 (sh), 2873 (sh), 1588 (vs), 1529 (sh), 1474 (s), 1428 (s), 1383 (m), 1304 (m), 1171 (vw), 1099 (w), 931 (w), 767 (vw), 606 (m) cm^{-1}. Commercially available ligands were used without further purification. Infrared spectra were recorded on a Perkin-Elmer Spectrum One spectrometer using KBr pellets in the region 4000–400 cm^{-1}. TGA/DTA measurements were carried out with a Mettler Toledo TGA/SDTA 851 under a stream of dry N$_2$ (60 mL min^{-1}) at a heating rate of 5 K min^{-1}. A Bandelin Sonorex RK-100H ultrasonic bath operating at 35 kHz with a maximum power output of 160 W was used for ultrasonic irradiation.

X-ray crystallography

Diffraction datasets for **1**, **3**, **4** and **5** were collected on a Bruker APEX II and for **2** on an Oxford Xcalibur CCD diffractometer, both equipped with graphite-monochromated Mo-K$_\alpha$ radiation. The summary of the data collection and the crystallographic parameters of compounds **1–4** are listed in Table 1. After collection and integration, the data were corrected for Lorentz and polarization effects. The structures were solved by direct methods and refined by full-matrix least squares on the weighted F^2 values for all reflections using the SHELX suite of programs.[20] All non-hydrogen atoms in clusters **1–5** were refined with anisotropic displacement parameters, except the minor position of disordered O- and C-type atoms. The hydrogen atoms were placed in fixed, idealized positions and refined as rigidly bonded to the corresponding atom. Some

Table 1 Crystal data and details of structural determination for **1–4**

	1	2	3	4
Empirical formula	C$_{62}$H$_{121}$Fe$_8$N$_5$O$_{35}$	C$_{48}$H$_{93}$Fe$_8$N$_{13}$O$_{27}$	C$_{55}$H$_{108}$Fe$_8$N$_{13}$O$_{27.5}$	C$_{42}$H$_{84}$Fe$_8$N$_{12}$O$_{24}$
M_r/g mol^{-1}	1943.44	1731.15	1838.34	1588.01
T/K	173(2)	293(2)	100(2)	100(2)
Wavelength/Å	0.71073	0.71073	0.71073	0.71073
Crystal system	Monoclinic	Cubic	Triclinic	Triclinic
Space group	$P2_1/n$	$Pa\bar{3}$	$P\bar{1}$	$P\bar{1}$
Unit cell dimensions				
a/Å	15.843(2)	24.0880(10)	13.2984(6)	13.616(5)
b/Å	20.180(3)	24.0880(10)	20.6844(9)	14.653(5)
c/Å	26.004(3)	24.0880(10)	29.1684(12)	18.767(6)
α/°	90	90	79.5700(10)	97.800(5)
β/°	91.680(2)	90	80.0600(10)	101.667(5)
γ/°	90	90	86.1600(10)	114.859(5)
V/Å^3	8310.5(18)	13976.62(10)	7767.0(6)	3222.8(19)
Z, ρ/Mg m^{-3}	4, 1.553	8, 1.645	4, 1.572	2, 1.636
μ/mm^{-1}	1.441	1.698	1.533	1.829
$F(000)$	4064	7168	3828	1640
Crystal size/mm^3	0.100 × 0.040 × 0.040	0.30 × 0.30 × 0.20	0.25 × 0.2 × 0.15	0.39 × 0.20 × 0.10
θ range for data collection/°	1.49–24.72	2.93–25.49	0.72–25.00	1.72–21.73
Index ranges	−18 ≤ h ≤ 18, −23 ≤ k ≤ 23, −30 ≤ l ≤ 30	−29 ≤ h ≤ 16, −28 ≤ k ≤ 29, −29 ≤ l ≤ 17	−15 ≤ h ≤ 15, −24 ≤ k ≤ 24, −34 ≤ l ≤ 34	−14 ≤ h ≤ 14, −15 ≤ k ≤ 15, −19 ≤ l ≤ 19
Reflections collected	63 708	34 700	84 329	24 639
Independent reflections	14 174 [R_{int} = 0.1212]	4344 [R_{int} = 0.0409]	27 350 [R_{int} = 0.0577]	7607 [R_{int} = 0.0889]
Completeness to θ_{max}	100.0%	99.8%	99.9%	99.8%
Data/restraints/parameters	14174/446/1049	4344/7/309	27350/54/1937	7607/19/810
Goodness-of-fit on F^2	1.001	1.003	1.013	1.000
Final R indices [$I > 2\sigma(I)$]: R_1, wR_2	0.0591, 0.1423	0.0355, 0.0900	0.0429, 0.0944	0.0457, 0.1060
R indices (all data): R_1, wR_2	0.1085, 0.1774	0.0533, 0.1000	0.0603, 0.1049	0.0779, 0.1219
Largest diff. peak, hole (e Å^{-3})	1.092, −0.898	0.345, −0.411	2.124, −1.960	0.714, −0.488

methyl groups of carboxylate ligands and alcohol groups of triethanolamine in **1–5** were found to be disordered; application of restraints provided reasonable geometrical parameters and thermal displacement coefficients. CCDC 1063435 (**1**), 1063436 (**2**), 1063437 (**3**), 1063438 (**4**), and 1063439 (**5**).

Magnetic measurements

Magnetic susceptibility data for **1–4** were obtained using a Quantum Design MPMS-5XL SQUID magnetometer. The polycrystalline samples were compacted and immobilized into cylindrical PTFE capsules. The data were acquired as a function of field and temperature. All data were corrected for the contribution of the sample holder (PTFE capsule) and the diamagnetic contributions of compounds **1–4** calculated from Pascal's constants using tabulated values (**1**: -1.22×10^{-8} m^3 mol^{-1}, **2**: -1.09×10^{-8} m^3 mol^{-1}, **3**: -1.16×10^{-8} m^3 mol^{-1}, **4**: -1.00×10^{-8} m^3 mol^{-1}).

Synthesis of [Fe$_8$O$_3$(O$_2$CCHMe$_2$)$_9$(tea)(teaH)$_3$]·MeCN·2(H$_2$O) (1). To a solution of **5** (0.094 g, 0.1 mmol) in 5 mL MeCN, triethanolamine (0.1 mL, 0.112 g, 0.75 mmol) and pyrazine (0.04 g, 0.5 mmol) were added. The resulting dark brown mixture was exposed to high intensity ultrasonic irradiation at 30 °C for 30 min. The brown crystals of **1** suitable for X-ray analysis were filtered off after one week, washed with acetonitrile and dried in air. Yield: 0.06 g, 69% (based on Fe). Elemental analysis calcd for C$_{62}$H$_{121}$Fe$_8$N$_5$O$_{35}$ (1943.4 g mol^{-1}): C, 38.08; H, 6.85; N, 3.58%. Found: C, 38.07; H, 6.31; N, 3.54%. IR (KBr pellet): ν = 3385 (br. m), 2965 (m), 2925 (m), 2870 (m), 1584 (vs), 1472 (s), 1428 (s), 1391 (m), 1375 (m), 1348 (m), 1304 (m), 1264 (m), 1169 (w), 1095 (s), 1030 (sh), 1004 (sh), 926 (m), 908 (m), 840 (w), 759 (w), 738 (w), 587 (m), 515 (m), 422 (m) cm^{-1}.

Synthesis of [Fe$_8$O$_3$(O$_2$CCHMe$_2$)$_6$(N$_3$)$_3$(tea)(teaH)$_3$] (2). Cluster **2** can be synthesized in different solvents and under different conditions.

Method A. In a typical experiment the mixture of **5** (0.094 g, 0.1 mmol), NaN$_3$ (0.022 g, 0.33 mmol) and teaH$_3$ (0.055 g, 0.36 mmol) in 10 mL EtOH (MeOH or 1 : 1 EtOH/CH$_2$Cl$_2$ could also be used) was heated at reflux for 60 min and then filtered. The filtrate was kept in a closed vial whose lid was pierced with several holes at room temperature. The black hexagonal crystals of **2** suitable for X-ray analysis were filtered off the next day, washed with hexane and dried in air. Yield: 0.045 g, 69% (based on Fe) in EtOH; 0.048 g (74%) in MeOH; 0.034 g (52%) in EtOH/CH$_2$Cl$_2$.

Method B. The mixture of **5** (0.094 g, 0.1 mmol), NaN$_3$ (0.024 g, 0.36 mmol) and teaH$_3$ (0.053 g, 0.35 mmol) in 10 mL EtOH was placed under ultrasonic irradiation for 32 min and then filtered. The filtrate was kept in a closed vial whose lid was pierced with several holes at room temperature. The black hexagonal crystals of **2** suitable for X-ray analysis were filtered off the next day, washed with hexane and dried in air. Yield: 0.045 g, 69%.

The identity of **2** prepared by methods A and B was established by comparison of IR data, elemental and TG analyses as well as by single-crystal X-ray diffraction analysis. Elemental analysis for **2** prepared by method A in EtOH, calcd for C$_{48}$H$_{93}$Fe$_8$N$_{13}$O$_{27}$ (1731.08 g mol^{-1}): C, 33.30; H, 5.41; N, 10.52%. Found: C, 33.56; H, 5.47; N, 10.23%. IR (KBr pellet): ν = 3416 (br. m), 2969 (m), 2925 (m), 2865 (m), 2068 (vs), 1577 (vs), 1471 (s), 1429 (s), 1391 (m), 1375 (sh), 1348 (sh), 1311 (m), 1098 (s), 1071 (m), 1038 (sh), 1004 (sh), 926 (sh), 909 (m), 875 (w), 579 (m), 515 (m), 414 (m) cm^{-1}.

Synthesis of [Fe$_8$O$_3$(O$_2$CCMe$_3$)$_6$(N$_3$)$_3$(tea)(teaH)$_3$]·0.5(EtOH) (3). A solution containing [Fe$_3$O(O$_2$CCMe$_3$)$_6$(H$_2$O)$_3$](Me$_3$CCO$_2$)· 2(Me$_3$CCO$_2$H) (0.23 g, 0.2 mmol), NaN$_3$ (0.038 g, 0.6 mmol) and teaH$_3$ (0.084 g, 0.6 mmol) in 10 mL EtOH was heated under reflux for 1 hour and then filtered. The filtrate was kept in a closed vial at room temperature. The next day, well-defined dark brown crystals of **3** suitable for X-ray analysis were filtered off, washed with EtOH and dried in air. Yield: 0.065 g, 47% (based on Fe). Elemental analysis calcd for C$_{55}$H$_{108}$Fe$_8$N$_{13}$O$_{27.5}$ (1838.28 g mol^{-1}): C, 35.93; H, 5.92; N, 9.90%. Found: C, 35.27; H, 5.73; N, 9.68%. IR (KBr pellet): ν = 3471 (br. m), 2959 (m), 2899 (m), 2871 (m), 2059 (vs), 1577 (vs), 1484 (s), 1458 (w), 1426 (s), 1378 (w), 1362 (m), 1265 (w), 1227 (m), 1087 (sh), 1041 (w), 910 (m), 787 (w), 741 (w), 603 (m), 516 (m), 426 (m) cm^{-1}.

Synthesis of [Fe$_8$O$_3$(O$_2$CCHMe$_2$)$_6$(N$_3$)$_3$(mdea)$_3$(MeO)$_3$] (4). The mixture of **5** (0.062 g, 0.07 mmol), NaN$_3$ (0.014 g, 0.21 mmol) and mdeaH$_2$ (0.100 g, 0.83 mmol) in 10 mL MeOH was exposed to high-intensity ultrasonic irradiation for 1 hour and then filtered. The orange solution was allowed to evaporate slowly at room temperature. Red-brown crystals suitable for single-crystal X-ray measurements were obtained after one week, washed with MeOH and dried in air. Yield: 0.015 g, 24% (based on Fe). Elemental analysis for C$_{42}$H$_{84}$Fe$_8$N$_{12}$O$_{24}$ (1588.01 g mol^{-1}): C, 31.76; H, 5.33; N, 10.58%. Found: C, 31.76; H, 5.29; N, 10.34%. IR data (KBr pellet): ν = 3431 (br. m), 2967 (m), 2921 (m), 2870 (m), 2811 (sh), 2068 (vs), 1578 (vs), 1472 (m), 1429 (s), 1375 (w), 1339 (w), 1291 (w), 1087 (m), 1053 (sh), 1001 (w), 903 (m), 877 (w), 761 (w), 628 (sh), 584 (m), 530 (m) cm^{-1}.

Results and discussion

Syntheses and preliminary characterization

For preparation of octanuclear iron(III) cluster **1**, [Fe$_8$O$_3$(O$_2$CCHMe$_2$)$_9$(tea)(teaH)$_3$]·MeCN·2(H$_2$O), an acetonitrile solution containing a smaller trinuclear iron(III) isobutyrate precursor [Fe$_3$O(O$_2$CCHMe$_2$)$_6$(H$_2$O)$_3$]NO$_3$·2(MeCN)·2(H$_2$O) (**5**), pyrazine and an excess of the teaH$_3$ ligand was exposed to ultrasonic irradiation at 35 kHz with a maximum power output of 160 W for 30 min. Storing this solution at room temperature gave ∼69% of well-defined brown crystals of **1** after one week. The use of some amount of pyrazine in the reactions was mandatory and afforded crystals of **1** suitable for single-crystal X-ray measurements. The inclusion of sodium azide in the reaction of trinuclear isobutyrate or pivalate Fe(III) clusters with teaH$_3$ gave octanuclear clusters [Fe$_8$O$_3$(O$_2$CCHMe$_2$)$_6$(N$_3$)$_3$-

(tea)(teaH)$_3$] (**2**) and [Fe$_8$O$_3$(O$_2$CCMe$_3$)$_6$(N$_3$)$_3$(tea)(teaH)$_3$]·0.5-(EtOH) (**3**). Thus, cluster **2** was prepared in approx. 70% yield in different solvent media such as EtOH, MeOH or a mixture of EtOH/CH$_2$Cl$_2$ under reflux or ultrasonic irradiation, whereas treatment of the trinuclear pivalate precursor with three equivalents of teaH$_3$ and three equivalents of sodium azide in refluxing EtOH gave octanuclear Fe^{III} pivalate cluster **3** in a lower (47%) yield. Clusters **2** and **3** have {Fe$_8$O$_3$} cores similar to that of **1**, where six carboxylate groups and four amino-alcohol ligands additionally bridge the iron atoms; these are differentiated from **1** by the replacement of three carboxylate ligands with three azide anions (Fig. 1b and c). Ultrasonic treatment of the Fe(III) trinuclear isobutyrate precursor **5** with an excess of mdeaH$_2$ and three equivalents of NaN$_3$ in MeOH gave cluster **4**, [Fe$_8$O$_3$(O$_2$CCHMe$_2$)$_6$(N$_3$)$_3$(mdea)$_3$(MeO)$_3$], in ~25% yield. Similar to **1–3**, the iron(III) atoms in the {Fe$_8$O$_3$} core of **4** are also connected by six carboxylate groups and three aminoalcohol ligands (mdea^{2-}), however three methoxide anions execute bridging functions (Fig. 1d) in place of the tetradentate tea^{3-} ligands in the aforementioned compounds.

The IR spectra of **1–4** display very strong and broad bands in the 1584–1577 cm^{-1} and 1429–1426 cm^{-1} regions that arise from the asymmetric and symmetric vibrations of the co-ordinated carboxylate groups, respectively. In the range of 2969–2865 cm^{-1} the C–H asymmetric and symmetric stretching vibrations for methyl groups of pivalates and isobutyrates are observed, while the asymmetric and symmetric bending vibrations for these methyl groups produce a strong single band in the region of 1484–1472 cm^{-1} and a doublet in the region of 1380–1340 cm^{-1}, respectively. The presence of solvate water (**1**) and ethanol (**3**) molecules, and OH groups of the doubly deprotonated teaH^{2-} ligands in **1**, **2** and **3**, caused the appearance of broad absorption bands in the region of 3471–3385 cm^{-1}. A very strong peak in the range of 2068–2059 cm^{-1} corresponds to the N≡N stretching vibrations of azide ligands in **2**, **3** and **4**.

Thermogravimetric analyses (TGA) for **1–4** were performed under a nitrogen atmosphere in the temperature range of 25–800 °C (Fig. S7–S10†). The TGA data show that the thermal decomposition of clusters **1–3** with triethanolamine ligands
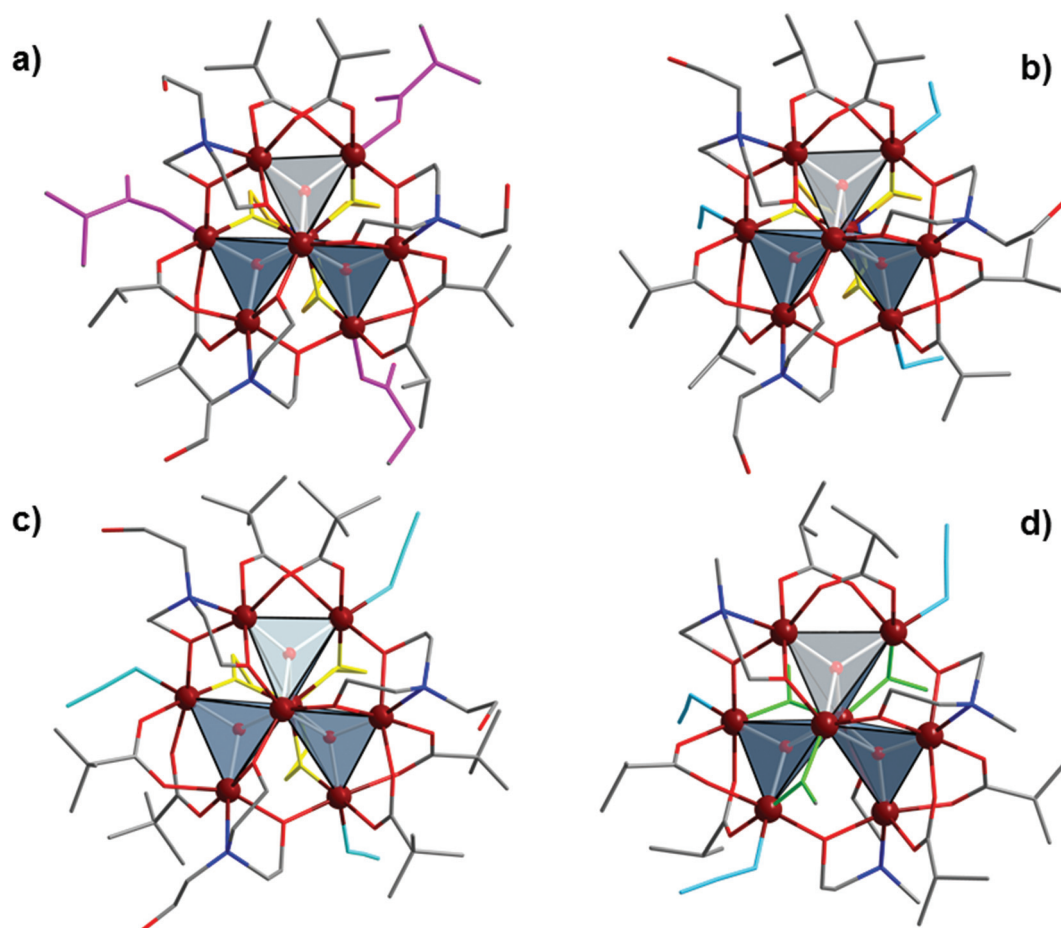

Fig. 1 Structures of the coordination clusters in **1** (a), **2** (b), **3** (c), and **4** (d). The propeller-shaped {Fe$_8$O$_3$} cores are highlighted as transparent grey polyhedra. Color codes: Fe, brown spheres; C, grey, N, blue, O, red sticks. In **1**, three monodentate isobutyrates are highlighted in pink, azide ligands in **1–3** shown as light blue sticks; a tridentate tea^{3-} ligand is shown in yellow (**1–3**); bridging methoxy groups in **4** are shown as green sticks. Hydrogen atoms and solvent molecules are omitted for clarity.

proceeds through several stages: the main weight loss steps of 64.3% (**1**), 59.4% (**2**) and 59.3% (**3**) take place between 100 and 450 °C; these correspond to removal of the organic groups of the clusters. The remaining organic ligands decomposed in one step within the range of 540–790 °C to the final metal oxide products. Cluster **1** loses the organic ligands (three molecules of the aminoalcohol ligand and nine pivalates) in two steps from 120 °C to 400 °C; the total first weight loss of 64.3% (calcd: 63.1%) is accompanied by an endothermic peak at 229 °C. The decomposition of the remaining tea^{3-} ligand takes place in the interval from 570 to 770 °C. Clusters **2** and **3** are stable up to 120 °C, and then they start to decompose in three weakly resolved steps until approx. 450 °C. The first two steps of the TGA curve of **2** are associated with an endothermic peak at 205 °C with a weight loss up to 230 °C; this corresponds to removal of the three azido groups and one carboxylate ligand (found: 13.8%; calcd: 12.3%). The third step for **2** is the loss of three teaH^{2-} and five isobutyric groups (found: 45.6%; calcd: 45.4%). Similar to **2**, cluster **3** in the temperature range of 120–225 °C exhibits a first weight loss of 8.9% (calcd: 8.1%) that indicates removal of the solvent (ethanol) molecule and three azido groups (exothermic effect at 220 °C). The next two steps correspond to the decomposition of four molecules of amino-alcohol ligands (one tea^{3-} and three teaH^{2-}) and four pivalates, for a total weight loss of 50.5% (calcd: 54.0%). After a plateau extending to 540 °C, further heating of **2** and **3** instigates a fourth weight loss of 8.1% (**2**) and 9.9% (**3**) until 630 °C, and this corresponds to removal of the remaining aminoalcohol ligand (calcd: 8.4% for **2** and 11.0% for **3**) to give the oxides with a total weight loss of 67.5% (**2**) and 69.2% (**3**) (calcd: 68.7% for **2** and 73.1% for **3**). The TGA data show that cluster **4** is the least stable compound. It remains stable up to 180 °C followed by the loss of all organics in three unresolved steps until ~400 °C, with a total weight loss of 57.9% (calcd: 61.1%) to the final metal oxides. The decomposition is accompanied by one exothermic peak at 234 °C and one endothermic peak at 279 °C.

Structural description

X-ray analysis showed that all compounds **1–4** contain octanuclear Fe^{III} clusters with propeller-shaped {Fe$_8$O$_3$} cores and disk outlines of ~1.6–1.7 nm diameter and ~1.2–1.5 nm thickness. The cluster compound [Fe$_8$O$_3$(O$_2$CCHMe$_2$)$_9$(tea)(teaH)$_3$]·MeCN·2(H$_2$O) (**1**) crystallizes in the space group $P2_1/n$, and [Fe$_8$O$_3$(O$_2$CCHMe$_2$)$_6$(N$_3$)$_3$(tea)(Htea)$_3$] (**2**) crystallizes in $Pa\bar{3}$ and resides on a three-fold axis, thus having the C_3 molecular symmetry, whereas [Fe$_8$O$_3$(O$_2$CCMe$_3$)$_6$(N$_3$)$_3$(tea)(Htea)$_3$]·0.5(EtOH) (**3**) and [Fe$_8$O$_3$(O$_2$CCHMe$_2$)$_6$(N$_3$)$_3$(mdea)$_3$(MeO)$_3$] (**4**) both crystallize in $P\bar{1}$. The asymmetric unit of **1** contains one Fe$_8$ cluster, one MeCN and two water molecules, while the asymmetric unit of **3** contains two crystallographically independent Fe$_8$ clusters and one solvent ethanol molecule as shown in Fig. S2 and S9,† respectively.

The propeller-shaped cores of these clusters have two central axial Fe^{III} ions that are bridged by three μ$_4$-O^{2-}; these further bridge two peripheral Fe^{III} ions to form one of the three blades of the propeller (Fig. 1 and S1†). These outer Fe pairs are not coplanar, and thus the outer six Fe ions do not form a flat wheel; they form two triangles that reside on two different parallel plains and separated by 1.709 Å in **2** or mutually inclined with dihedral angles of 2.43° in **1**, 5.31° and 3.51° in **3**, and 2.55° in **4**. The central pair of iron ions represents the axle of the propeller with the shortest Fe···Fe distances of 2.897(1) Å in **1**, 2.873(6) Å in **2**, 2.895(7) Å and 2.911(8) Å in **3**, and 2.792(2) Å in **4**. The distances between the central and peripheral Fe atoms range from 2.962(1) to 3.133(1) Å in **1**, from 2.988(6) to 3.139(6) Å in **2**, from 2.962(8) to 3.139(7) Å in **3** and from 2.990(2) to 3.077(2) Å in **4**. Additionally, in **1–3** the Fe^{III} ions are bridged by four triethanolamine ligands: three doubly deprotonated (teaH^{2-}) and one triply deprotonated (tea^{3-}), and also carboxylate groups (pivalates in **1** and **3**, and isobutyrate in **2**). In **4**, eight Fe^{III} atoms are furthermore bridged by three fully deprotonated N-methyldiethanolamine, six isobutyrate groups, and three methoxide anions. Three monodentate pivalate ligands in **1** and three azide ligands in **2–4** complete the coordination spheres of three outer Fe^{III} atoms. The replacement of these monodentate ligands might permit further linkage to form higher dimensionality clusters and cluster-based polymeric networks.[18]

In clusters **1–4**, each Fe atom is in the +3 oxidation state (BVS, 2.711–3.197 (Table S1†)) and has a distorted octahedral geometry. The axial Fe^{III} ions are all O$_6$-coordinated: for **1–3** one of the axial Fe^{III} atoms is coordinated by three μ$_4$-oxo atoms and three oxygen atoms from three triethanolamine ligands; whereas another Fe^{III} atom is bonded to three μ$_4$-oxo atoms and three oxygen atoms from one triply deprotonated tea^{3-}. In cluster **4**, one of the central Fe^{III} atoms is capped by three μ$_4$-O^{2-} atoms, two alkoxide O atoms from two mdea^{2-} and a methoxide O atom, while another central Fe^{III} via three μ$_4$-O^{2-} atoms, one alkoxide O atom from mdea^{2-} and two methoxide O atoms. The six peripheral Fe^{III} atoms in **1** have different coordination environments: three Fe atoms have an O$_6$ donor set being coordinated by a μ$_4$-O^{2-} atom, three O atoms from two bridging and one monodentate carboxylates and two O atoms from one doubly deprotonated (teaH^{2-}) and one triply deprotonated (tea^{3-}) ligand, while the other three metal atoms each have an O$_5$N donor set arising from one μ$_4$-O^{2-} atom, two O atoms from two bridging pivalates, and two O atoms and one N atom from one teaH^{2-}. In clusters **2–4**, the six peripheral iron atoms all have an O$_5$N coordination environment. For **2** and **3**, the O$_5$N coordination geometries for three peripheral Fe^{III} atoms arise from a μ$_4$-oxygen atom, two O atoms from two polyalcohol ligands, two O atoms from two carboxylate groups and one N atom from azide; the remaining peripheral Fe^{III} atoms are each ligated by a μ$_4$-oxygen atom, two O atoms from one doubly deprotonated polyalcohol ligand, two O atoms from two carboxylate groups and one N atom from the same teaH^{2-}. In cluster **4**, three Fe^{III} atoms are each coordinated by a μ$_4$-oxygen atom, two O atoms from two bridging carboxylate groups, an O atom from a mdea^{2-} ligand, an O atom of the MeO$^-$ group and a N atom from azide; the remaining three Fe^{III} atoms are each co-

ordinated by a μ_4-oxygen atom, two O atoms from two bridging carboxylate groups, and two O atoms from a mdea^{2-} ligand. All of the Fe–O bond distances in **1–4** are in the range of 1.900(4)–2.313(2) Å (Fe–μ_4-O: 1.916(4)–2.313(2) Å, Fe–O$_{carb}$: 1.935(2)–2.106(2) Å, and Fe–O$_{alc}$: 1.900(4)–2.013(4) Å). The Fe–N$_{azide}$ distances (only in **2–4**) range from 2.021(6) to 2.089(3) Å, whereas the Fe–N$_{alc}$ distances are distinctly longer, 2.205(5)–2.357(3) Å (Table 2).

Table 2   Selected bond distances (Å) for **1–4**

1

Fe1–O28	1.934(4)	Fe3–O33	1.961(4)	Fe5–O20	1.958(5)	Fe7–O8	1.958(4)
Fe1–O25	1.936(4)	Fe3–O2	1.976(4)	Fe5–O31	1.969(4)	Fe7–O32	1.971(4)
Fe1–O22	1.945(4)	Fe3–O14	1.976(4)	Fe5–O26	1.986(4)	Fe7–O23	1.977(5)
Fe1–O1	2.049(4)	Fe3–O29	1.987(4)	Fe5–O3	1.998(4)	Fe7–O1	1.996(4)
Fe1–O2	2.055(4)	Fe3–O11	2.037(5)	Fe5–O17	2.043(5)	Fe7–O4	2.049(5)
Fe1–O3	2.115(4)	Fe3–O13	2.063(5)	Fe5–O19	2.095(4)	Fe7–O6	2.056(5)
Fe2–O32	1.929(4)	Fe4–O3	1.933(4)	Fe6–O1	1.940(4)	Fe8–O2	1.954(4)
Fe2–O31	1.936(4)	Fe4–O28	1.978(4)	Fe6–O25	1.972(4)	Fe8–O22	1.966(4)
Fe2–O33	1.938(4)	Fe4–O29	1.980(4)	Fe6–O26	1.990(4)	Fe8–O23	1.978(5)
Fe2–O3	2.183(4)	Fe4–O18	2.002(5)	Fe6–O7	2.007(5)	Fe8–O12	1.986(5)
Fe2–O2	2.210(4)	Fe4–O16	2.044(5)	Fe6–O5	2.043(4)	Fe8–O10	2.054(5)
Fe2–O1	2.233(4)	Fe4–N3	2.292(5)	Fe6–N2	2.294(5)	Fe8–N1	2.285(5)

2

Fe1–O6$^{\#1}$	1.937(2)	Fe2–O8$^{\#1}$	1.945(2)	Fe3–O1	1.943(2)	Fe4–O6	1.984(2)
Fe1–O6$^{\#2}$	1.937(2)	Fe2–O8	1.945(2)	Fe3–O2	1.985(2)	Fe4–O7$^{\#2}$	1.992(2)
Fe1–O6	1.937(2)	Fe2–O8$^{\#2}$	1.945(2)	Fe3–O8	1.992(2)	Fe4–O1	2.007(2)
Fe1–O1$^{\#1}$	2.198(2)	Fe2–O1$^{\#1}$	2.075(2)	Fe3–O7	2.007(2)	Fe4–O5	2.030(2)
Fe1–O1$^{\#2}$	2.198(2)	Fe2–O1	2.075(2)	Fe3–O4	2.049(2)	Fe4–N3	2.050(3)
Fe1–O1	2.198(2)	Fe2–O1$^{\#2}$	2.075(2)	Fe3–N2	2.273(3)	Fe4–O3	2.106(2)

3

Fe1–O25	1.943(2)	Fe5–O2	1.974(2)	Fe9–O44	1.942(2)	Fe13–O54	1.967(2)
Fe1–O27	1.956(2)	Fe5–O19	1.977(2)	Fe9–O47	1.946(2)	Fe13–O43	1.990(3)
Fe1–O26	1.962(3)	Fe5–O25	1.991(2)	Fe9–O49	1.958(2)	Fe13–O29	1.993(2)
Fe1–O3	2.142(2)	Fe5–N7	2.030(3)	Fe9–O29	2.060(2)	Fe13–O35	2.031(3)
Fe1–O1	2.186(2)	Fe5–O7	2.048(3)	Fe9–O30	2.073(2)	Fe13–N21	2.043(3)
Fe1–O2	2.313(2)	Fe5–O5	2.077(3)	Fe9–O28	2.074(2)	Fe13–O37	2.083(3)
Fe2–O23	1.927(3)	Fe6–O3	1.961(2)	Fe10–O54	1.937(2)	Fe14–O29	1.936(2)
Fe2–O17	1.935(2)	Fe6–O19	1.981(2)	Fe10–O52	1.941(2)	Fe14–O47	1.980(2)
Fe2–O20	1.959(3)	Fe6–O20	1.985(2)	Fe10–O53	1.952(3)	Fe14–O38	1.983(3)
Fe2–O2	2.045(2)	Fe6–O8	2.008(3)	Fe10–O30	2.153(2)	Fe14–O46	2.000(3)
Fe2–O3	2.051(2)	Fe6–O10	2.041(3)	Fe10–O28	2.208(2)	Fe14–O36	2.061(3)
Fe2–O1	2.134(2)	Fe6–N2	2.272(3)	Fe10–O29	2.257(2)	Fe14–N15	2.257(3)
Fe3–O27	1.971(2)	Fe7–O26	1.974(3)	Fe11–O52	1.992(2)	Fe15–O53	1.964(2)
Fe3–O16	1.980(2)	Fe7–O22	1.987(3)	Fe11–O50	1.993(2)	Fe15–O46	1.977(3)
Fe3–O1	1.983(2)	Fe7–O3	2.004(2)	Fe11–O28	2.010(2)	Fe15–O30	1.989(2)
Fe3–O15	2.048(3)	Fe7–O11	2.025(3)	Fe11–N18	2.025(3)	Fe15–O39	2.026(3)
Fe3–N4	2.060(3)	Fe7–N10	2.058(4)	Fe11–O31	2.039(3)	Fe15–O41	2.042(3)
Fe3–O13	2.066(3)	Fe7–O9	2.075(3)	Fe11–O33	2.071(2)	Fe15–N24	2.089(3)
Fe4–O2	1.939(2)	Fe8–O1	1.933(2)	Fe12–O28	1.942(2)	Fe16–O30	1.954(2)
Fe4–O16	1.980(2)	Fe8–O22	1.970(3)	Fe12–O34	1.987(3)	Fe16–O50	1.963(2)
Fe4–O17	1.981(3)	Fe8–O23	1.987(3)	Fe12–O43	1.988(3)	Fe16–O49	2.004(2)
Fe4–O4	2.002(3)	Fe8–O12	2.021(3)	Fe12–O44	1.993(2)	Fe16–O40	2.012(3)
Fe4–O6	2.032(3)	Fe8–O14	2.043(3)	Fe12–O32	2.039(3)	Fe16–O42	2.021(3)
Fe4–N1	2.299(3)	Fe8–N3	2.291(3)	Fe12–N14	2.258(3)	Fe16–N16	2.357(3)

4

Fe1–O26	1.912(4)	Fe3–O18	1.985(4)	Fe5–O25	1.995(4)	Fe7–O3	1.924(4)
Fe1–O19	1.920(4)	Fe3–O24	2.013(4)	Fe5–O20	2.005(4)	Fe7–O23	1.978(4)
Fe1–O21	1.944(4)	Fe3–O1	2.018(4)	Fe5–N7	2.021(6)	Fe7–O22	1.992(4)
Fe1–O1	2.059(4)	Fe3–O17	2.020(5)	Fe5–O2	2.023(4)	Fe7–O13	2.010(4)
Fe1–O2	2.122(4)	Fe3–N4	2.026(6)	Fe5–O9	2.036(4)	Fe7–O11	2.056(5)
Fe1–O3	2.129(4)	Fe3–O15	2.033(4)	Fe5–O7	2.057(4)	Fe7–N3	2.205(5)
Fe2–O24	1.900(4)	Fe4–O2	1.926(4)	Fe6–O3	1.916(4)	Fe8–O26	1.988(4)
Fe2–O22	1.943(4)	Fe4–O18	1.986(4)	Fe6–O21	1.978(4)	Fe8–O23	2.005(4)
Fe2–O25	1.947(4)	Fe4–O6	2.001(5)	Fe6–O20	1.996(4)	Fe8–O14	2.017(5)
Fe2–O2	2.070(4)	Fe4–O19	2.004(4)	Fe6–O10	2.008(4)	Fe8–N10	2.038(6)
Fe2–O1	2.078(4)	Fe4–O8	2.041(4)	Fe6–O12	2.050(4)	Fe8–O1	2.040(4)
Fe2–O3	2.124(4)	Fe4–N1	2.223(5)	Fe6–N2	2.212(5)	Fe8–O16	2.052(4)

#1 y, z, x, #2 z, x, y.

Table 3 Hydrogen bonds in **1–3** [Å and °]

D–H⋯A	d(D–H)	d(H⋯A)	d(D⋯A)	∠(DHA)
1				
O35–H35E⋯O30	0.87	1.98	2.757(10)	149.0
O35–H35D⋯O27[#1]	0.87	1.969	2.836(11)	175.0
O34–H34B⋯O15	0.90	1.995	2.873(11)	164.0
O34–H34A⋯O35[#2]	0.88	1.89	2.765(15)	174.0
O30–H30A⋯O15[#3]	0.82	1.90	2.717(8)	172.8
O27–H27⋯O34[#4]	0.84	1.88	2.703(14)	166.8
O24–H24⋯O21[#4]	0.82	1.95	2.752(7)	167.0

#1 $-x + 1$, $-y + 1$, $-z + 1$, #2 $-x + 1/2$, $y + 1/2$, $-z + 1/2$, #3 $-x + 1/2$, $y - 1/2$, $-z + 1/2$, #4 $-x + 3/2$, $y - 1/2$, $-z + 1/2$.

2				
O9–H9⋯N3[#3]	0.82	2.10	2.868(6)	156.0

#3 x, $-y + 1/2$, $z - 1/2$.

3				
O51–H51⋯N6[#1]	0.84	1.93	2.758(5)	168.1
O48–H48⋯N24[#2]	0.84	2.06	2.883(4)	167.4
O45–H45⋯O55[#3]	0.84	1.89	2.707(5)	162.8
O24–H24⋯N10[#3]	0.90	1.95	2.825(5)	163.1
O21–H21⋯N23	0.84	2.08	2.871(5)	155.6
O18–H18⋯N26[#4]	0.84	2.08	2.900(5)	165.3
O55–H55⋯O51[#5]	0.84	1.85	2.692(5)	178.8

#1 $x + 1$, y, $z - 1$, #2 $-x + 1$, $-y$, $-z$, #3 $-x + 1$, $-y + 1$, $-z + 1$ #4 $x - 1$, y, $z + 1$, #5 x, y, $z + 1$.

The presence of the uncoordinated alkoxide groups of teaH^{2-} in **1–3** and N-containing azide ligands in **2** and **3**, as well as solvate molecules (H$_2$O in **1** and an ethanol molecule in **3**), results in the formation of hydrogen-bonded networks in **1–3** (Table 3). In cluster **1**, two solvate water molecules (O34 and O35) form an O–H⋯O hydrogen bond of 2.762(14) Å with each other and several intermolecular hydrogen bonds of 2.696(13)–2.840(11) Å with the uncoordinated alkoxide groups from the neighboring clusters to generate a 3D hydrogen-bonded network. Some additional contacts between uncoordinated carboxylate oxygens of monodentate pivalates and the uncoordinated protonated alkoxide oxygens are also presented (Table 3). In cluster **2**, a 3D hydrogen-bonded network is formed by the intermolecular O–H⋯N contacts of 2.868(6) Å between alkoxide oxygens of teaH^{2-} and N atoms from azide ligands. For cluster **3**, the two crystallographically independent clusters form five O–H⋯N hydrogen bonds of 2.758(5)–2.900(5) Å between their uncoordinated alcohol groups (O18, O21, O24 atoms from one cluster and O48 and O51 atoms from another one) and nitrogen atoms of azides from the neighboring clusters (N26 [$x - 1$, y, $z + 1$], N23, N10 [$-x + 1$, $-y + 1$, $-z + 1$], N24 [$-x + 1$, $-y$, $-z$], and N6 [$x + 1$, y, $z - 1$] atoms, respectively) to generate a 2D layer as shown in Fig. S5.† The remaining protonated oxygen atom (O45) of the teaH^{2-} ligand forms a short hydrogen bond of 2.707(5) Å with the oxygen atom (O55 [$-x + 1$, $-y + 1$, $-z + 1$]) of an ethanol molecule; and finally the solvate EtOH molecules connect the adjacent layers into a 3D network through O–H⋯O hydrogen bonds (O55–H55⋯O51 [x, y, $z + 1$] of 2.692(5) Å).

Magnetic properties

The low-field temperature-dependent magnetic susceptibility data of **1–4** are depicted in Fig. 2 as open circles. Since the
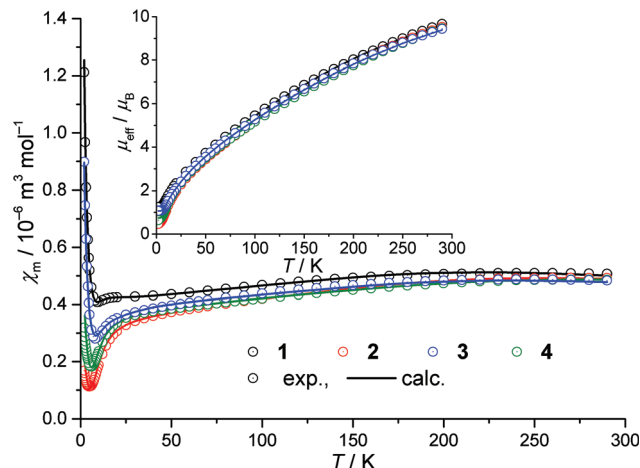

Fig. 2 Temperature dependence of the magnetic susceptibility χ_m of **1–4** at 0.1 Tesla; inset: temperature dependence of the corresponding effective magnetic moment μ_{eff}.

compounds feature comparable structures, the data exhibit common trends. For each of the four compounds, the effective magnetic moment approaches approximately $\mu_{eff} = 9.6\mu_B$ at 290 K (Fig. 2, inset) which is well below the spin-only value of $16.7\mu_B$ expected for eight non-interacting high-spin Fe^{III} centers, thus indicating that the antiferromagnetic exchange interactions are dominant within each compound. In addition, the effective magnetic moments continuously decrease by lowering the temperature; this is consistent with the dominating antiferromagnetic interactions. For **1–4**, when decreasing the temperature from 150 K to approximately 10 K, χ_m decreases as expected for antiferromagnetic exchange interactions. For even lower temperatures, all χ_m curves exhibit minima and subsequent increasing values that reveal either paramagnetic impurities, minor ferromagnetic interaction contributions or a combination of both.

Due to computational limitations (the Hilbert space dimension for the eight spin-5/2 centers amounts to 6^8) several approximations are required to model the magnetic data of compounds **1–4**. Although exhibiting different (distorted octahedral) ligand-field environments, each of the eight Fe^{III} centers is treated as an effective $S = 5/2$ center due to the energy splitting of their 3d^5 systems. Thus, their exchange interactions are described by an effective isotropic Hamiltonian including a g-value of $g_{eff} = 2$. Since **1–4** are each composed of eight centers, the total number of exchange interaction parameters J_{ij} is 28 $((n - 1)n/2)$. To reduce the number of independent parameters, the computer program wxJFinder[10,12] has been used to determine which of the interactions are negligible or may be treated as identical. Adopting the ideas of Weihe and Güdel[13a] as well as Werner et al.,[13b] the calculations of wxJFinder are based on the angular overlap model (AOM) taking into account various experimental datasets for compounds containing oxo-bridged Fe^{III} centers. Therefore, these calculations deliver the expected ranges for the exchanged interaction parameters based upon structural information.

Due to the similar structures of **1**–**3**, the simulated exchange parameters differ by small amounts from one compound to another. Therefore, the coupling scheme that is applied in the fit to the effective spin Hamiltonian is explained using the example of compound **3**. The calculations of wxJFinder show that 15 of the 28 exchange interaction parameters are negligible. 12 of the remaining 13 parameters are divided into four categories, each represented by three (almost) identical parameters. Thus, all compounds are described by effective Hamiltonians that contain five independent exchange parameters J_i as depicted in Fig. 3 (notation: $\hat{H}_{ex} = \sum_{k<l} -2J_i \cdot \hat{S}_k \cdot \hat{S}_l$).

From a magnetochemical perspective, compound **4** is different from **1**–**3** in that a single azide and a single amine ligand exchange places, leading to a different set of exchange paths and parameters: J_1, J_2 and J_3 describe the exchange interactions as in **1**–**3**, while J_5 represents the interaction between the two neighboring Fe^{III} centers that both feature amine ligands. J_6 is the corresponding interaction between the two adjacent Fe^{III} centers that are ligated by azides, and the remaining four interactions (two neighboring centers featuring an azide and an amine ligand, respectively) are all reproduced by J_4.

The parameters calculated by wxJFinder are employed as initial values for the corresponding fit of the effective Hamiltonian to the magnetic susceptibility data. These fits are performed by the computer program CONDON 2.0.[11] They result in exchange interaction parameters which differ from the calculated initial values by 8 cm^{-1} or less. A possible paramagnetic impurity is included in the model by the equation $\chi_{m,meas} = (1 - \rho)\chi_{m,comp} + 8\rho\chi_{m,pm}$ where $\chi_{m,meas}$ is the measured molar magnetic susceptibility, and $\chi_{m,comp}$ and $\chi_{m,pm}$ are the susceptibilities of a compound and of a single spin-5/2 center, respectively.

The resulting fit parameters are shown in Table 4 and the corresponding curves as straight lines in Fig. 2. According to the Heisenberg model employed here, all compounds are characterized by a single ferromagnetic (J_1) and otherwise antiferromagnetic independent exchange interaction parameters J_i. An analysis of the correlation coefficients for the various J_i pairs derived from the least-squared fit parameters (Tables

Table 4 Magnetochemical analysis details of **1**–**4**

	1	2	3	4
g_{eff}	2	2	2	2
J_1/cm^{-1}	+35.8 ± 0.2	+25.3 ± 1.3	+44.1 ± 0.1	+16.0 ± 1.1
J_2/cm^{-1}	−22.8 ± 3.4	−22.0 ± 2.2	−22.3 ± 0.2	−17.5 ± 0.2
J_3/cm^{-1}	−22.6 ± 2.9	−22.0 ± 2.2	−22.3 ± 0.2	−17.0 ± 0.7
J_4/cm^{-1}	−14.7 ± 0.6	−16.4 ± 0.2	−18.6 ± 0.4	−11.8 ± 0.5
J_5/cm^{-1}	−8.5 ± 0.6	−6.1 ± 0.2	−7.9 ± 0.3	−38.1 ± 5.0
J_6/cm^{-1}	N/A	N/A	N/A	−7.5 ± 0.3
ρ/%	0.58 ± 0.01	0.11 ± 0.01	0.41 ± 0.01	0.19 ± 0.01
SQ^a	0.6%	1.5%	1.4%	1.6%

^{a} The goodness-of-fit parameter SQ is defined as: $SQ = \sqrt{\dfrac{1}{n}\sum_{i=1}^{n}\dfrac{\left(\chi_{exp}(i) - \chi_{calc}(i)\right)^2}{\chi_{exp}^2(i)}}$.

S2–S5†) indicates that J_1 generally displays the most pronounced correlation with the other exchange energies, and the evolution of the remaining J_i parameters as well as the goodness-of-fit are highlighted in Fig. S18–S21† for an artificial modification of J_1 by ±10%. Compounds **1**–**3** show comparable sets of parameters due to their similar structures, while **4** reveals slightly lower magnitude exchange interactions, along with the different coupling schemes along the propeller tips. The compounds are characterized by moderate antiferromagnetic interactions along the edges and weaker antiferromagnetic interactions at the tips. Consistent with the expectation of the superexchange mechanism, a moderate ferromagnetic interaction is found along the axis between the most proximal Fe^{III} atoms within the compounds since they form, in combination with their bridging oxo ligands, approximately right-angled triangles. Note that the effect of this exchange interaction (J_1) competes with the contribution of paramagnetic impurities, thus these modeled values exhibit potentially larger uncertainties than the standard deviations given in Table 4. On the other hand, the structures of **1**, **2** and **4** contain one cluster site while **3** shows alternating crystallographically distinct cluster sites, twisted by 180° with respect to one another, and thus the behavior of **3** might be influenced by further effects. Nevertheless, for all of these complexes wxJFinder calculates parameters of the same signs and comparable values. The introduction of azide ligands mainly influences the exchange pathways if these ligands are not symmetrically distributed over the structure as can be deduced from the different parameter sets found for **4** in comparison to **1**–**3**. The calculated ground state of all compounds corresponds to an $S = 0$ effective spin state in agreement with the low value of μ_{eff} at 290 K. Higher energy states are calculated according to the best fit parameters. In part, they are shown in Fig. S12–S15† for the lower energy range (0–420 cm^{-1}) shifted relative to the ground state. The first excited state for **1**–**4** corresponds to an effective $S = 1$ state in the range of 21–24 cm^{-1}. Finally, we note that a further reduction in the number of independent exchange energies (J_i) by one (assuming the most similar exchange energies, J_2 and J_3 to be equal)
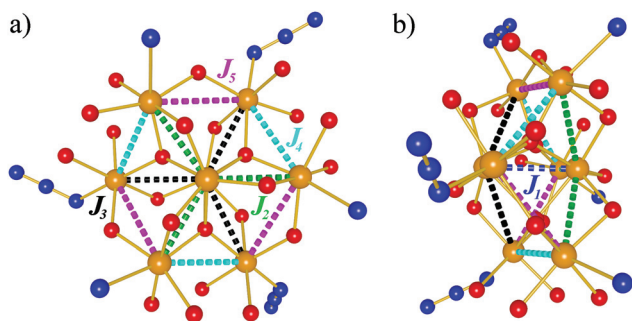

Fig. 3 Coupling scheme of **1**–**3** using the example of compound **3**: (a) front view, (b) side view. Fe^{III} atoms are shown as yellow spheres, O atoms as red balls, and N atoms as blue balls.

significantly decreases the fit quality, with SQ increasing by approx. 0.5 (**1**) to 1.0% (**4**), see also Fig. S16 and S17.†

A comparison of the presented fit parameters to those of similar compounds is limited, since the exchange interaction parameters for compounds composed of eight oxo-bridged Fe^{III} centers are not reported in the literature[16–19,21] so far. However, magnetic susceptibility data and the $S = 0$ ground state are consistent with the results of these studies. Slightly smaller compounds as the disc-like structures containing seven oxo-bridged Fe^{III} centers have been analysed in more detail.[16,17,21] Mukherjee *et al.*[21] reported J values which were calculated by applying the formula of Weihe and Güdel[13a] for Fe^{III} dimers. These exchange interaction parameters are thus in the same range as the starting parameters for J_2–J_5 (J_6) calculated by wxJFinder. Further analysis to estimate the quality of the calculated J, *e.g.* a calculation of $\chi_m T$ *vs.* T and a subsequent comparison to the presented experimental $\chi_m T$ *vs.* T data, was omitted.[21]

Conclusions

In summary, a combined approach has been used to determine reasonable exchange energies in a series of octanuclear propeller-like Fe^{III} clusters that feature distorted hexagonal-bipyramidal Fe_8 polytopes of isotropic spin-5/2 centers, featuring up to six types of magnetic exchange coupling pathways. The title compounds with the formulae $[Fe_8O_3(O_2CCHMe_2)_9(tea)(teaH)_3]\cdot MeCN\cdot 2(H_2O)$ (**1**), $[Fe_8O_3(O_2CCHMe_2)_6(N_3)_3(tea)(teaH)_3]$ (**2**), $[Fe_8O_3(O_2CCMe_3)_6(N_3)_3(tea)(teaH)_3]\cdot 0.5(EtOH)$ (**3**), and $[Fe_8O_3(O_2CCHMe_2)_6(N_3)_3(mdea)_3(MeO)_3]$ (**4**) were prepared by direct reaction of oxo-centered trinuclear carboxylate precursors with triethanolamine or *N*-methyldiethanolamine. The challenge central to the magnetochemical modeling, namely overcoming the overparameterization issues associated with reproducing the susceptibility data *via* a Heisenberg–Dirac–van Vleck model Hamiltonian with multiple exchange energies J, here employed the semi-empirical program wxJFinder that predicts the exchange energies for the Fe–O–Fe pathways. Importantly, wxJFinder can be used to determine which of these interactions are negligible or may be treated as identical, thus effectively reducing the number of independent fitting parameters. The parameters calculated by wxJFinder are employed as initial values for the corresponding fit of the effective Hamiltonian to the magnetic susceptibility data. The magnetochemical studies showed that for **1–4**, antiferromagnetic exchange interactions dominate along the edges of the propeller while a moderate ferromagnetic interaction is found along the propeller axis.

Acknowledgements

Notes and references

1 *Magnetism: Molecules to Materials III. Nanosized Magnetic Materials*, ed. J. S. Miller and M. Drillon, Wiley-VCH, 2002, 400pp.

2 I. L. Malaestean, A. Ellern, S. Baca and P. Kögerler, *Chem. Commun.*, 2012, **48**, 1499.

3 I. L. Malaestean, M. Speldrich, A. Ellern, S. G. Baca and P. Kögerler, *Dalton Trans.*, 2011, **40**, 331.

4 I. L. Malaestean, M. Speldrich, A. Ellern, S. G. Baca and P. Kögerler, *Polyhedron*, 2010, **29**, 1990.

5 (*a*) T. C. Stamatatos, D. Foguet-Albiol, W. Wernsdorfer, K. A. Abboud and G. Christou, *Chem. Commun.*, 2011, **47**, 274; (*b*) D. Foguet-Albiol, K. A. Abboud and G. Christou, *Chem. Commun.*, 2005, 4282; (*c*) M. Murugesu, W. Wernsdorfer, K. A. Abboud and G. Christou, *Angew. Chem., Int. Ed.*, 2005, **44**, 892; (*d*) D. Foguet-Albiol, T. A. O'Brien, W. Wernsdorfer, B. Moulton, M. J. Zaworotko, K. A. Abboud and G. Christou, *Angew. Chem., Int. Ed.*, 2005, **44**, 897.

6 P.-H. Lin, S. Eastman, A. Bhatti, M. Brulotte, T. J. Burchell, I. Korobkov, G. Enright, R. Clérac and M. Murugesu, *Inorg. Chim. Acta*, 2011, **375**, 187.

7 (*a*) L. M. Wittick, B. Moubaraki, S. R. Batten, L. Spiccia, K. J. Berry and K. S. Murray, *Dalton Trans.*, 2004, 1003; (*b*) L. M. Wittick, L. F. Jones, P. Jensen, B. Moubaraki, L. Spiccia, K. J. Berry and K. S. Murray, *Dalton Trans.*, 2006, 1534; (*c*) S. Langley, K. J. Berry, B. Moubaraki and K. S. Murray, *Dalton Trans.*, 2009, 973; (*d*) S. K. Langley, B. Moubaraki, K. Berry and K. S. Murray, *Dalton Trans.*, 2010, 4848; (*e*) S. K. Langley, N. F. Chilton, M. Massi, B. Moubaraki, K. Berry and K. S. Murray, *Dalton Trans.*, 2010, 7236; (*f*) S. K. Langley, N. F. Chilton, B. Moubaraki and K. S. Murray, *Dalton Trans.*, 2012, 1033.

8 (*a*) A. Baniodeh, I. J. Hewitt, V. Mereacre, Y. Lan, G. Novitchi, C. E. Anson and A. K. Powell, *Dalton Trans.*, 2011, **40**, 4080; (*b*) V. Mereacre, D. Prodius, Y. Lan, C. Turta, C. E. Anson and A. K. Powell, *Chem. – Eur. J.*, 2011, **17**, 123.

9 Y.-F. Zeng, X. Hu, L. Xue, S.-J. Liu, T.-L. Hu and X.-H. Bu, *Inorg. Chem.*, 2012, **51**, 9571.

10 S. G. Baca, T. Secker, A. Mikosch, M. Speldrich, J. van Leusen, A. Ellern and P. Kögerler, *Inorg. Chem.*, 2013, **52**, 4154.

11 (*a*) M. Speldrich, H. Schilder, H. Lueken and P. Kögerler, *Isr. J. Chem.*, 2011, **51**, 215; (*b*) J. van Leusen, M. Speldrich, H. Schilder and P. Kögerler, *Coord. Chem. Rev.*, 2015, **289–290**, 137; see also http://www.condon.fh-aachen.de/.

12 J. van Leusen and P. Kögerler, wxJFinder 1.1, RWTH Aachen University, 2013, http://wxjfinder@ac.rwth-aachen.de.

13 (*a*) H. Weihe and H. U. Güdel, *J. Am. Chem. Soc.*, 1997, **119**, 6539; (*b*) R. Werner, S. Ostrovsky, K. Griesar and W. Haase, *Inorg. Chim. Acta*, 2001, **326**, 78.

14 N. V. Gerbeleu, A. S. Batsanov, G. A. Timko, I. T. Struchkov, K. M. Indrichan and G. A. Popovich, *Dokl. Akad. Nauk SSSR*, 1987, **293**, 364.

15 M. Murugesu, K. A. Abboud and G. Christou, *Dalton Trans.*, 2003, 4552.

16 L. F. Jones, P. Jensen, B. Moubaraki, K. J. Berry, J. F. Boas, J. R. Pilbrow and K. S. Murray, *J. Mater. Chem.*, 2006, **16**, 2690.

17 A. M. Ako, O. Waldmann, V. Mereacre, F. Klöwer, I. J. Hewitt, C. E. Anson, H. U. Güdel and A. K. Powell, *Inorg. Chem.*, 2007, **46**, 756.

18 T. Liu, Y.-J. Zhang, Z.-M. Wang and S. Gao, *J. Am. Chem. Soc.*, 2008, **130**, 10500.

19 I. A. Gass, C. J. Milios, A. Collins, F. J. White, L. Budd, S. Parsons, M. Murie, S. P. Perlepes and E. K. Brechin, *Dalton Trans.*, 2008, 2043.

20 G. M. Sheldrick, *Acta Crystallogr., Sect. A: Fundam. Crystallogr.*, 2008, **64**, 112.

21 S. Mukherjee, R. Bagai, K. A. Abboud and G. Christou, *Inorg. Chem.*, 2011, **50**, 3849.